Flexible FET-Type VEGF Aptasensor Based on Nitrogen-Doped Graphene Converted from Conducting Polymer

Oh Seok Kwon,[†,§] Seon Joo Park,[†,§] Jin-Yong Hong,[†] A-Reum Han,[‡] Jun Seop Lee,[†] James S. Lee,[†] Joon Hak Oh,[‡,*] and Jyongsik Jang[†,*]

[†]World Class University Program of Chemical Convergence for Energy & Environment, School of Chemical and Biological Engineering, Seoul National University, Seoul 151-742, Korea, and [‡]School of Nano-Bioscience and Chemical Engineering, KIER-UNIST Advanced Center for Energy, Low Dimensional Carbon Materials Center, Ulsan National Institute of Science and Technology, Ulsan 689-798, Korea. [§]These authors contributed equally to this work.

ABSTRACT Graphene-based field-effect transistors (FETs) have been developed rapidly and are currently considered as an alternative for postsilicon electronics. In this study, polypyrrole-converted nitrogen-doped few-layer graphene (PPy-NDFLG) was grown on Cu substrate by chemical vapor deposition combined with vapor deposition polymerization and then transferred onto a flexible substrate. Furthermore, antivascular endothelial growth factor (VEGF) RNA aptamer conjugated PPy-NDFLG was integrated into a liquid-ion gated FET geometry to fabricate a high-performance VEGF aptamer-based sensor. Field-induced high sensitivity was observed for the analyte-binding events, eventually leading to the recognition of the target molecules at an unprecedentedly low concentration (100 fM). Additionally, the aptasensor had excellent reusability, mechanical bendability, and durability in the flexible process. The developed methodology describes, for the first time, the fabrication of N-doped graphene using conducting polymers including heteroatoms in their structures as the carbonization precursor and demonstrates its use in a high-performance, flexible FET-type aptasensor to detect vascular endothelial growth factor as a cancer biomarker.

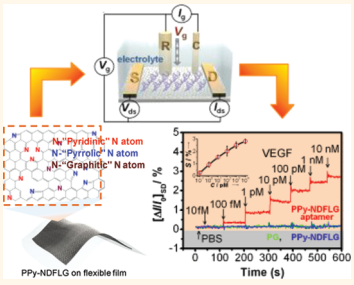

KEYWORDS: nitrogen-doped graphene · field-effect transistor · conducting polymer · aptasensor · vascular endothelial growth factor · aptamer

Graphene is a single-atom-thick, sp^2-carbon-based material that has attracted significant interest recently owing to its excellent electrical, optical, and mechanical properties.[1−5] The extraordinary charge carrier mobility of graphene holds great promise for nanoscale applications such as electronic devices, energy storage, solar cells, display devices, and chemical/biological sensors.[6−10] However, its applications, particularly in switching devices, are handicapped by the absence of a band gap in the intrinsic form.[11−13] Various approaches including nanoribbons and nanomesh have been developed to open or tune an energy gap in graphene and improve the semiconducting properties.[14,15] One of the more feasible ways to control the semiconducting properties of graphene is the doping approach, which is a common method for tailoring the electronic properties of a semiconductor material.[16−20] Theoretical and experimental studies on graphene doping have demonstrated the possibility of opening the band gap and modulating conducting types by substituting carbon atoms with foreign atoms, leading to a metal-semiconductor transition. Recently, a number of approaches such as chemical vapor deposition (CVD) with heteroatom gases, arc-discharge, and adsorbate-induced doping have been proposed to synthesize nitrogen-doped graphene.[21−38] Nevertheless, most of these approaches are limited by the use of gaseous raw materials at a high temperature for a long time as well as complex pre/post-treatments.

Recently, angiogenesis, the formation of new blood vessels sprouting from the preexisting vasculature, has been studied at the molecular mechanism level because it is an important factor related to the metastasis and growth of human tumors.[39] Although various proangiogenic factors such as platelet-derived growth factor (PDGF) and basic fibroblast growth factor (bFGF) are demonstrated, the vascular endothelial growth factor (VEGF) family is the predominant proangiogenic factor.[39,40] Vascular endothelial growth factor potently promotes angiogenesis by activating VEGF-receptors and is indispensable for vascular development, resulting in this being an attractive target for controlling the angiogenic factor. Therefore, vascular endothelial growth factor discrimination in blood is useful for the early diagnosis, staging, and monitoring of cancers. From this point of view, a few

* Address correspondence to jsjang@plaza.snu.ac.kr; joonhoh@unist.ac.kr.

Received for review November 13, 2011 and accepted January 7, 2012.

Published online January 08, 2012
10.1021/nn204395n

significant techniques for detecting vascular endothelial growth factor levels in blood have been proposed.[41−45] However, all of these methods (or recognition processes) still require rapid detection and high sensitivity for further improvement.

Herein, we have developed, for the first time, the concept that conducting polymers including heteroatoms in their structures can be utilized as the carbon source for fabricating doped graphene. We report the facile fabrication of polypyrrole-converted nitrogen-doped few-layer graphene (PPy-NDFLG) and describe its integration with an anti-VEGF RNA aptamer into a flexible field-effect transistor (FET) platform suitable for electronic control. Field-induced high sensitivity was observed for the analyte-binding events, eventually leading to the recognition of the target molecules at an unprecedentedly low concentration. Additionally, the aptamer-based sensor (aptasensor) showed enhanced reusability through a recycle assay and also had excellent mechanical bendability and durability in the flexible system. To our knowledge, this is the first demonstration of a flexible FET-type aptasensor using nitrogen-doped graphene to detect vascular endothelial growth factor as a cancer biomarker.

RESULTS AND DISCUSSION

Fabrication of PPy-NDFLG. Previously, we synthesized N-doped carbon nanomaterials converted from various conducting polymer nanomaterial precursors through a carbonization process.[46−48] Continuous, few-layer, N-doped graphene was grown on 25-μm-thick Cu foil by CVD using polypyrrole as the solid precursor.[1−3] Figure 1 shows a schematic representation of the experimental process for the fabrication of PPy-NDFLG. First, 1 wt % $CuCl_2$ solution (as an initiator) was deposited by spin coating (at 7000 rpm for 30 s) on the Cu substrate. For vapor deposition polymerization (VDP), the reactor containing the $CuCl_2$/Cu substrate was evacuated at room temperature until the internal pressure reached about 1 Torr and was put in the system under a static vacuum. Then, liquid-phase pyrrole monomers were introduced into the reactor by injection and completely vaporized by heating the reactor to 70 °C. The vaporized pyrrole monomers were contacted with Cu cations and polymerized *via* chemical oxidation polymerization on the Cu substrate. The thickness of the PPy film was approximately 20 nm.[49] PPy-NDFLG was successfully obtained by optimizing the CVD experimental parameters (temperature profile, precursor and gas flow rates, and system pressure), as shown in the inset of Figure 1, and subsequently transferred onto a flexible and transparent polyethylene naphthalate (PEN) film (see Supporting Information Figure S1).

Characterization of PPy-NDFLG. To confirm N-doping of PPy-NDFLG, X-ray biomarker spectroscopy (XPS)

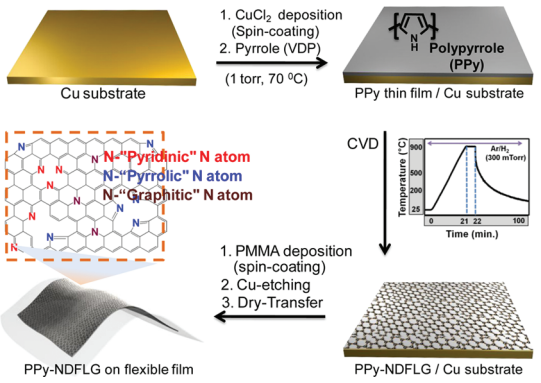

Figure 1. Synthetic protocol of PPy-NDFLG on flexible substrate.

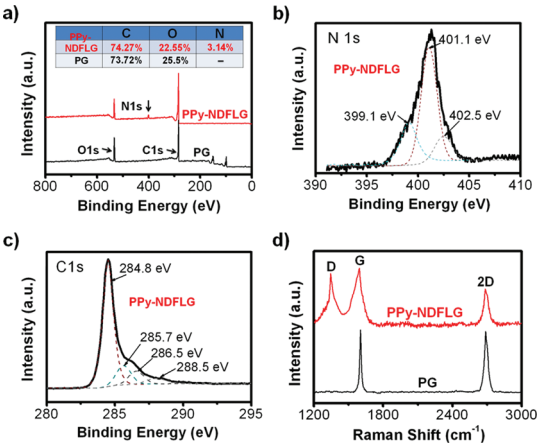

Figure 2. (a) XPS spectra of the PG and PPy-NDFLG. (b) XPS N 1s spectrum and (c) XPS C 1s spectrum of PPy-NDFLG. (d) Raman spectra of PPy-NDFLG and PG composed of two layers.

studies were carried out. Figure 2 presents the typical XPS and Raman spectra results of PPy-NDFLG and pristine graphene (PG) as a control, grown with gases (as carbon precursors) on the Cu surface (see Supporting Information Figures S2 and S3). The survey scan spectrum from the XPS analysis shows the presence of the principal C1s, O1s, and N1s core levels, with no evidence of impurities, whereas the N1s peak is absent in the PG (Figure 2a). The N1s peak is observed clearly in the PPy-NDFLG and had three components centered at 399.1, 401.1, and 402.5 eV, corresponding to pyridinic-N, pyrrolic-N, and graphitic-N, respectively (Figure 2b). The C1s core level peaks could be resolved into three components centered at ~284.8, 285.7, and 286.5 eV, representing sp^2C-sp^2C, $N-sp^2C$, and $N-sp^3C$ bonds. The C1 peak at 288.5 eV was also attributed to a CO-type bond (Figure 2c). The O1s peak was observed in all samples, due to physisorbed oxygen on the graphene surface.[15−20]

Raman measurements are an effective tool for demonstrating the doping effect and the layer number of graphene through the 2D/G height ratio because the G and 2D peaks have different doping dependences.[50]

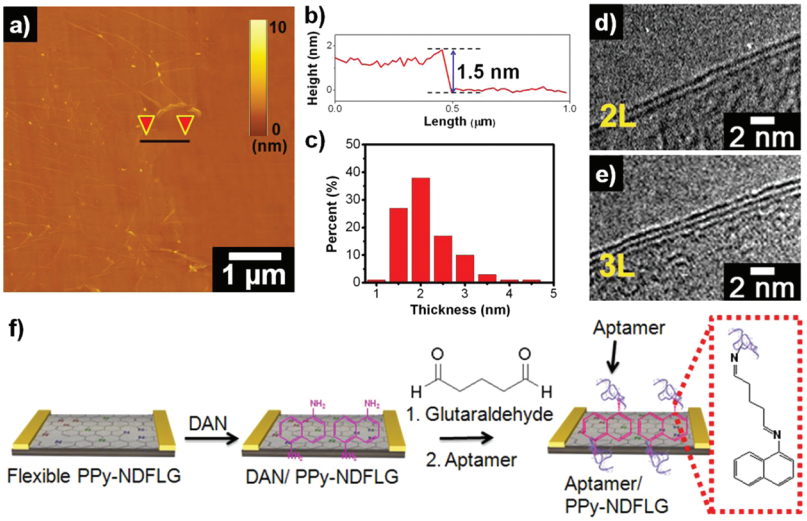

Figure 3. (a) High-magnification atomic force microscopy (AFM) image of PPy-NDFLG on a silicon substrate. The black line indicates a scanning trace of the PPy-NDFLG, which is plotted in (b). (c) Histogram of the average graphene thickness data collected from 100 PPy-NDFLGs samples. It shows that the majority of the PPy-NDFLG is a few layers. (d and e) HR-TEM images of PPy-NDFLG. (f) Schematic illustration of reaction steps for the fabrication of aptasensor platforms based on PPy-NDFLG conjugated with anti-VEGF RNA aptamer.

Figure 2d displays the Raman spectra of PPy-NDFLG and PG (bilayer) samples. The most characteristic feature of PPy-NDFLG was the presence of the D-band in the Raman spectra. As shown in Figure 2d, the D peak (~1356 cm^{-1}) in PPy-NDFLG was clearly visible, indicative of the presence of significant defects compared to PG: such defects are usually generated during heteroatom doping.[50−52] These defects may be induced by the disordered structures and vacancies in the graphene lattice by nitrogen doping. As nitrogen atoms become doped into the graphene layers, the D peak intensity increases rapidly and the 2D (~2697 cm^{-1}) decreases monotonically. More importantly, the 2D to G intensity ratio in PPy-NDFLG (I_{2D}/I_G = 0.832) is lower than that in PG (I_{2D}/I_G = 0.926). The widths of the D, G, and 2D peaks in PPy-NDFLG are broader than those of PG, which can also be ascribed to various bonding structures and defects after doping.[29,30] Therefore, as compared with PG, the intensities of the D, G (~1587 cm^{-1}), and 2D bands in PPy-NDFLG indicate that most of them consist of N-doped graphene.[52] The few-layer characteristic was confirmed by high-magnification AFM analysis (Figure 3a), where the cross-sectional analysis showed a vertical distance of *ca.* 1.5 nm (Figure 3b). The average thickness of PPy-NDFLG at 100 randomly chosen samples was found to be *ca.* 2 nm (Figure 3c). In addition, the HR-TEM images also reveal two- to three-layer graphene (Figure 3d and e), which is consistent with the results of AFM analysis.

Fabrication of the Aptasensor. To utilize PPy-NDFLG as a signal transducer in the electronic aptamer-based sensor system, we introduced an aptamer that can bind to a wide variety of entities with high selectivity, specificity, and affinity. A small aptamer also allows innovative recognition of binding-induced label-free detection between transducers and analytes in FET-type aptasensors.[53−57] Therefore, anti-VEGF RNA aptamer immobilization was performed by modifying the side plane of PPy-NDFLG with glutaraldehyde-conjugated 1,5-diaminonaphthalene (DAN) through a Schiff-base reaction in pure environments (Figure 3f). The DAN component was bound to the PPy-NDFLG through $\pi-\pi$ stacking between the pyrenyl group and the plane of graphene.[58] The Schiff-base reaction proceeded through chemical attachment between the amine group of the aptamer and the aldehyde group of glutaraldehyde connected at the DAN/PPy-NDFLG/PEN film.[59] To evaluate the quality of the electrical contact after introduction of the anti-VEGF RNA aptamer, the current−voltage ($I-V$) characteristics were measured at each process stage. Figure 4a exhibits $I-V$ curves of DAN/PPy-NDFLG without aptamer and PPy-NDFLG-aptamer on the flexible substrate. The difference of the dI/dV values is presumably due to the difference in the resistance, and the $I-V$ curves show linear behaviors. This result demonstrates that the immobilization of the aptamer on the PPy-NDFLG resulted in a reliable electrical contact. Moreover, as shown in the AFM image of Figure S4 in the Supporting Information, the length of the anti-VEGF RNA aptamer was *ca.* 2 nm, which might induce the recognition binding events within the Debye length of the double layer.[53−57] Accordingly, when the PPy-NDFLG-aptamer is assembled between source and drain electrodes, the binding of vascular endothelial growth factor to the aptamer can be demonstrated by observing a change in current output through the FET devices.

Electrical Properties and Real-Time Responses of the FET-Type Aptasensor. To investigate the electrical characteristics of the aptasensor, we fabricated liquid-ion gated FETs

with phosphate-buffered solution (PBS, pH 7.5).[58−63] Figure 4b outlines the experimental setup used to evaluate the performance of the aptasensor into a liquid-ion gated FET in pure environments. The aptasensor fabricated was assessed using more than 10 devices under ambient conditions to show distinguishing features in comparison with PG. Figure 4c demonstrates the output characteristics of the aptasensor, which operates at room temperature, under various gate voltages (V_g). For PG devices, the drain-to-source current (I_{ds}) became more negative with negatively increasing V_g, indicating p-type (hole-transporting) behavior due to the absorption of oxygen or water in air (see Supporting Information Figure S5),[4−8] whereas for PPy-NDFLG-aptamer, I_{ds} could be positively enhanced with positively increasing V_g, meaning that the stable n-type (electron-transporting) behavior took place after nitrogen doping.[23] The vascular endothelial growth factor biomolecule is bound to the specific anti-VEGF RNA aptamer, which in turn transduces a signal in the FET-type aptasensor. Such aptamer/VEGF interactions can affect the charge-carrier density on the surface of PPy-NDFLG, and thus it may allow label-free recognition of target molecules on the FET configuration. To identify the sensing performance of the aptasensor, the I_{ds} was monitored in real time at constant V_{ds} = 50 mV (V_g = 0.05 V, a low operating voltage), upon the addition of various vascular endothelial growth factor concentrations. Figure 4d displays the real-time responses of PG, PPy-NDFLG without aptamer, and PPy-NDFLG-aptamer. The aptasensor showed a concentration-dependent increase in I_{ds} when it was exposed to the target molecules (VEGF), while no significant changes in the signals were observed for the PG and PPy-NDFLG without aptamer. This is presumably due to the Debye shielding effect of vascular endothelial growth factor or the surface of PPy-NDFLG in the electrolyte.[64−66] The current increase is due to the accumulation of negative charge carriers elicited by the aptamer−VEGF binding event. Specifically, the isoelectric point (p*I*) of vascular endothelial growth factor is 8.5, so the vascular endothelial growth factor will be positively charged under the experimental condition of pH 7.5. These positively charged vascular endothelial growth factor molecules can effectively screen the negative charges in the aptamer by deriving a structure deformation of aptamer, and then the VEGF−aptamer binding event can induce positive point charges in the liquid-ion gate

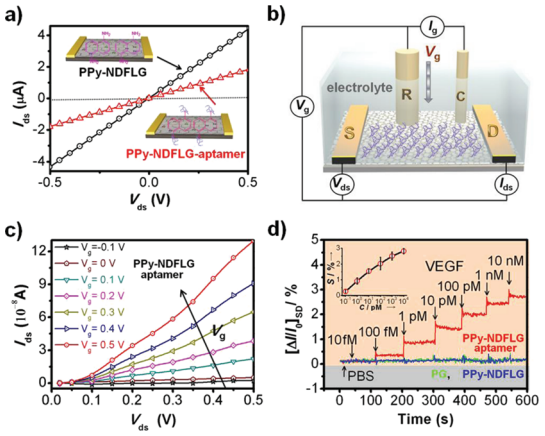

Figure 4. (a) Current−voltage curves of PPy-NDFLG on the PEN film before and after aptamer immobilization in air (V_{ds} = −0.5 V to +0.5 V and scan rate was 10 mV s^{-1}). (b) Schematic diagram of a liquid-ion gated FET using aptamer-conjugated PPy-NDFLG (Ag/AgCl reference electrode, R; platinum counter electrode, C; source and drain electrodes, S and D). (c) I_{ds}−V_{ds} output characteristics of PPy-NDFLG-aptamer at different V_g from −0.1 to 0.5 V in a step of 0.1 V in phosphate-buffered solution (V_{ds}, 0 to 0.5 V in a step of 50 mV). (d) Real-time responses and a calibration curve (*S* in the inset indicates $\Delta I/I_0$) of aptasensor with various vascular endothelial growth factor concentrations.

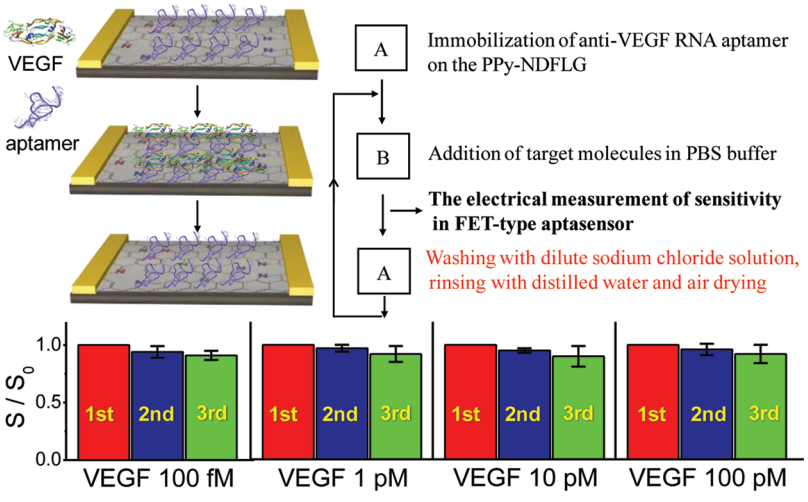

Figure 5. Reusability of aptasensor three times through a recycle process, which consists of three steps: washing with dilute 10% NaCl, rinsing with diethylpyrocarbonate-treated water, and air-drying (S/S_0, where S_0 is the initial sensitivity change and *S* is the measured sensitivity change after a reusable process).

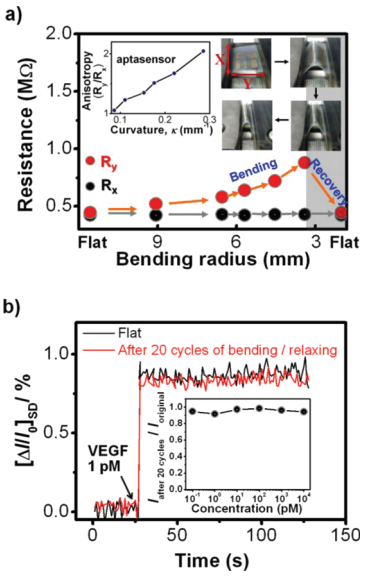

Figure 6. (a) Variation in resistance of a flexible aptasensor based on PPy-NDFLG-aptamer for different bending radii, which was adjusted by changing the distances in the holding direction: the left inset shows the anisotropy (R_y/R_x) in resistances measured perpendicular (R_x) and parallel (R_y) to the bending direction, *y*. The right inset displays the bending process. (b) Sensing behavior of the aptasensor toward 1 pM vascular endothelial growth factor after 20 cycles of bending/relaxing. The inset indicates a fatigue test toward various VEGF concentrations.

dielectric near the PPy-NDFLG, leading to the accumulation of negative charge carriers in the PPy-NDFLG channel. The increased positive gate voltage by the vascular endothelial growth factor binding event results in the increase of the I_{ds} of n-type PPy-NDFLG. This is similar to an n-type doping effect acting indirectly on the liquid-ion gate dielectric, rather than affecting directly the semiconducting layer.[67−69] The aptasensor showed a rapid response time of less than 1 s. The sensitivity change (*S*) was observed with the linear curve (Figure 4d, inset). Importantly, the minimum detection level was found to be *ca.* 100 fM (signal-to-noise: 3.1), approximately 1−3 orders of magnitude lower than that of conventional VEGF sensors.[35−38,67−69] Moreover, the aptasensor showed excellent selectivity toward bovine serum albumin solution (Figure S6).

Reusability of the Aptasensor. The aptasensor can be repeatedly utilized with various concentrations of the target molecules under a reusable recycle process. Figure 5 displays the schematic recycle process, and the sensitivity changes were calculated three times at various concentrations of VEGF (100 fM, 1 pM, 10 pM, and 100 pM). The recycle process is composed of three steps: (i) immobilization of the aptamer on FET substrate, (ii) injection of VEGF molecule into the aptasensor, (iii) washing with dilute sodium chloride solution and air drying. The aptasensor showed an efficient reusability with various VEGF concentrations by regenerating the aptamer in 10% NaCl solution. Although the sensitivity decreased slightly due to aptamer degradation (~5%), this result indicates that the aptasensor is highly reproducible and reusable.

Mechanical Properties of the Aptasensor. There has been a great deal of interest in the interaction of ultrasensitive semiconductors on plastic substrates owing to their excellent physical properties such as biocompatibility, flexibility, and light weight.[70,71] This is also a challenging area in chemical and biological sensors, especially for portable, wearable, or even implantable sensors. In this system, the FET-type aptasensor showed bendable flexibility on the PEN films. To manifest the mechanical flexibility of the aptasensor, the foldability of the flexible aptasensor substrate was examined by measuring resistances with respect to bending radii (Figure 6a). The resistances showed little variation up to a bending radius of *ca.* 9 mm, and the original resistance could be restored even for a bending radius of *ca.* 3 mm, demonstrating mechanical stability compared to conventional materials. Lastly, a fatigue test was conducted for the above aptasensor device. Figure 6b displays the typical change in response intensity after repeated bending/relaxing. The sensing behavior decreased slightly (<5%) in sensitivity after 20 bending cycles (Figure 6b, inset). These results clearly indicate that the aptasensor has excellent mechanical bending ability and durability, opening up the possibility of fabricating reliable flexible biosensors after further optimization.

CONCLUSION

In summary, we developed a new methodology for synthesizing PPy-NDFLG through VDP/CVD methods, and it was utilized as a signal transducer in a liquid-ion gated FET-type aptasensor to detect vascular endothelial growth factor, which plays a pivotal role in tumor growth and metastasis. The aptasensor displayed a rapid response time, ultrasensitivity, and efficient reusability. Moreover, the aptasensor also exhibited outstanding mechanical flexibility. From the viewpoint of its unprecedented sensing performance, PPy-NDFLG may offer a wide range of applications in biomedical diagnostics and environmental monitoring.

MATERIALS AND METHODS

Materials. Pyrrole (98%), copper(II) chloride (97%), 1,5-diaminonaphthalene, and glutaraldehyde were purchased from Aldrich. Vascular endotherlial growth factor ($VEGF_{165}$; MW = 38.2 kDa, p*I* = 8.5) was purchased from Cell Signal Technology, Inc. Anti-VEGF RNA aptamer was purchased from Bioneer Co. (Deajeon, Korea). The aptamer was modified at the 5′-terminus with an amino group, and its sequence was as follows: 5′-NH_2-AUG CAG

UUU GAG AAG UCG CGC AU-3′. The aptamer stock solution was diluted with diethylpyrocarbonate-treated water and stored in the freezer before use (−20 °C).

Fabrication of PPy-NDFLG. Polypyrrole thin film was formed by the VDP of pyrrole monomer on a $CuCl_2$-coated Cu foil and subsequently used as the solid carbon source. The 1 wt % $CuCl_2$ solution (500 μL) was first coated by a spin-coating method (7000 rpm for 30 s) on 25 μm thick Cu foils. The $CuCl_2$/Cu substrate was placed in a reactor. The internal pressure reached 1 Torr for the vaporization of monomer, and 0.18 mmol of pyrrole monomer was injected into the reactor. The VDP proceeded at 70 °C for 60 min. Subsequently, PPy-NDFLG was grown on a Cu substrate in a hot wall furnace. A typical growth process flow is as follows: (1) The PPy thin film/Cu substrate was loaded, hydrogen was added, the temperature was raised to 900 °C, and H_2 and Ar gas pressure at 300 mTorr under 10 and 50 sccm flows was maintained; (2) the PPy-NDFLG was grown for a desired period of time (*ca*. 1 min) when the temperature reached 900 °C; (3) after the growth of PPy-NDFLG, the furnace was cooled to room temperature. The Cu substrate was removed by immersing in copper etchant. Finally, the PPy-NDFLG was transferred to the flexible PEN film.

Fabrication of the Aptasensor Platform. To construct the liquid-ion gated FET-type aptasensor platform, in the first stage the gold electrode ($W/L = 20$; $L = 100$ μm channel length) was deposited on the PPy-NDFLG/PEN film by thermal evaporation. This FET substrate was treated with 10 μM 1,5-diaminonaphthalene in methanol (40 μL) for 1 h and then washed with distilled water. Subsequently, the immobilization of anti-VEGF RNA aptamer (1 pM, 40 μL) was carried out through the Schiff-base method after using 2% glutaraldehyde (20 μL) in PBS for 2 h and then rinsing with PBS solution.

Instrumentation. All electrical measurements were conducted with a Keithley 2400 sourcemeter and a Wonatech WBCS 3000 potentiostat. A solution chamber (200 μL volume) was designed and used for solution-based measurements. The current change was normalized as $\Delta I/I_0 = (I - I_0)/I_0$, where I_0 is the initial current and I is the measured value in real time, respectively. Raman spectra were collected with a LabRam Aramis (Horiba Jobin Yvon). The 514.5 nm line of an Ar ion laser was used as the excitation source, and a low power (<0.5 mW) was used to avoid unintentional heating.

Supporting Information Available: Additional information about sample preparation, characterization, and physicochemical properties, measurements of sensor performances, TEM, and AFM. This material is available free of charge *via* the Internet at http://pubs.acs.org.

Acknowledgment. This work was supported by World Class University (WCU) Program, National Research Foundation of Korea (NRF) grant funded by the Ministry of Education, Science and Technology (MEST) (R31-10031, 2011-0026424, 2011-0017174, 2011-0017125) and Global Frontier Research Center for Advanced Soft Electronics.

REFERENCES AND NOTES

1. Novoselov, K. S.; Geim, A. K.; Morozov, S. V.; Jiang, D.; Katsnelson, M. I.; Grigorieva, I. V.; Dubonos, S. V.; Firsov, A. A. Two-Dimensional Gas of Massless Dirac Fermions in Graphene. *Nature* **2005**, *438*, 197–200.
2. Li, X.; Cai, W.; An, J.; Kim, S.; Nah, J.; Yang, D.; Piner, R.; Velamakanni, A.; Tutuc, E.; Banerjee, S. K.; *et al*. Large-Area Synthesis of High-Quality and Uniform Graphene Films on Copper Foils. *Science* **2009**, *324*, 1312–1314.
3. Bhaviripudi, S.; Jia, X.; Dresselhaus, M. S.; Kong, J. Role of Kinetic Factors in Chemical Vapor Deposition Synthesis of Uniform Large Area Graphene Using Copper Catalyst. *Nano Lett* **2010**, *10*, 4128–4133.
4. Sun, Z.; Yan, Z.; Yao, J.; Beitler, E.; Zhu, Y.; Tour, J. M. Growth of Graphene from Solid Carbon Sources. *Nature* **2010**, *468*, 549–551.
5. Yang, W.; Ratinac, K. R.; Ringer, S. P.; Thordarson, P.; Gooding, J.; Braet, F. Carbon Nanomaterials in Biosensors: Should You Use Nanotubes or Graphene? *Angew. Chem., Int. Ed.* **2010**, *49*, 2114–2138.
6. Shin, K.-Y.; Hong, J.-Y.; Jang., J. Micropatterning of Graphene Sheets by Inkjet Printing and Its Wideband Dipole-Antenna Application. *Adv. Mater.* **2011**, *23*, 2113–2118.
7. Wu, J.; Pisula, W.; Mullen, K. Graphene as Potential Material for Electronics. *Chem. Rev.* **2007**, *107*, 718–747.
8. Wei, D.; Liu, Y. Controllable Synthesis of Graphene and Its Application. *Adv. Mater.* **2010**, *22*, 3225–3241.
9. Zhang, C.; Yuan, Y.; Wang, Y.; Liu, Z. Biosensing Platform Based on Fluorescence Resonance Energy Transfer from Upconverting Nanocrystals to Graphene Oxide. *Angew. Chem., Int. Ed.* **2011**, *50*, 6851–6854.
10. Myung, S.; Solanki, A.; Kim, K. S.; Lee, K.-B. Graphene-Encapsulated Nanoparticle-Based Biosensor for the Selective Detection of Cancer Biomarkers. *Adv. Mater.* **2011**, *23*, 2221–2225.
11. Rao, C. N. R.; Sood, A. K.; Subrahmanyam, K. S.; Govindaraj, A. Graphene: The New Two-Dimensional Nanomaterial. *Angew. Chem., Int. Ed.* **2009**, *48*, 7752–7777.
12. Allen, M. J.; Tung, V. C.; Kaner, R. B. Honeycomb Carbon: A Review of Graphene. *Chem. Rev.* **2010**, *110*, 132–145.
13. Heller, I.; Chatoor, S.; Mannik, J.; Zevenbergen, M. -A. G.; Dekker, C.; Lemay, S. G. Influence of Electrolyte Composition on Liquid-Gated Carbon Nanotube and Graphene Transistors. *J. Am. Chem. Soc.* **2010**, *132*, 17149–17156.
14. Rafiee, M. A.; Lu, W.; Thomas, A.; Zandiatashbar, V.; Rafiee, A.; Tour, J.; Koratkar, J. M.; Graphene Nanoribbon, N. A. Composites. *ACS Nano* **2010**, *4*, 7415–7421.
15. Song, L. L.; Zheng, X. H.; Wang, R. L.; Zeng, Z. Dangling Bond States, Edge Magnetism, and Edge Reconstruction in Pristine and B/N-Terminated Zigzag Graphene Nanoribbons. *J. Phys. Chem. C* **2010**, *114*, 12145–12150.
16. Li, Y.; Zhou, Z.; Shen, P.; Chen, Z. Spin Gapless Semiconductor−Metal−Half-Metal Properties in Nitrogen-Doped Zigzag Graphene Nanoribbons. *ACS Nano* **2009**, *3*, 1952–1958.
17. Wang, Y.; Shao, Y.; Matson, D. W.; Li, J.; Lin, Y. Nitrogen-Doped Graphene and Its Application in Electrochemical Biosensing. *ACS Nano* **2010**, *4*, 1790–1798.
18. Zhang, C.; Fu, L.; Liu, N.; Liu, M.; Wang, Y.; Liu, Z. Synthesis of Nitrogen-Doped Graphene Using Embedded Carbon and Nitrogen Sources. *Adv. Mater.* **2011**, *23*, 1020–1024.
19. Panchakarla, L. S.; Subrahm-anyam, K. S.; Saha, S. K.; Govindaraj, A.; Krishnamurthy, H. R.; Waghmare, U. V.; Rao, C. N. R. Synthesis, Structure, and Properties of Boron- and Nitrogen-Doped Graphene. *Adv. Mater.* **2009**, *21*, 4726–4730.
20. Ci, L.; Song, L.; Jin, C.; Wu, D.; Li, Y.; Srivastava, A.; Wang, Z. F.; Storr, K.; Balicas, L.; Liu, F.; *et al*. Atomic Layers of Hybridized Boron Nitride and Graphene Domains. *Nat. Mater.* **2010**, *9*, 430–435.
21. Martins, T.; Miwa, R.; da Silva, A. J. R.; Fazzio, A. Electronic and Transport Properties of Boron-doped Graphene Nanoribbons. *Phys. Rev. Lett.* **2007**, *98*, 196803.
22. Lin, Y.-C.; Lin, C.-Y.; Chin, P.-W. Controllable Graphene N-doping with Ammonia Plasma. *Appl. Phys. Lett.* **2010**, *96*, 133110.
23. Wang, X.; Li, X.; Zhang, L.; Yoon, Y.; Weber, P. K.; Wang, H.; Guo, H.; Dai, H. N-Doping of Graphene through Electrothermal Reactions with Ammonia. *Science* **2009**, *324*, 768–771.
24. Dong, X.; Fu, D.; Fang, W.; Shi, Y.; Chen, P.; Li, L.-J. Doping Single-Layer Graphene with Aromatic Molecules. *Small* **2009**, *5*, 1422–1426.
25. Qu, L.; Liu, Y.; Baek, J.-B.; Dai, L. Nitrogen-Doped Graphene as Efficient Metal-Free Electrocatalyst for Oxygen Reduction in Fuel Cells. *ACS Nano* **2010**, *4*, 1321–1326.
26. Li, X.; Wang, H.; Robison, J. T.; Sanchez, H; Diankov, G.; Dai, H. Simultaneous Nitrogen Doping and Reduction of Graphene Oxide. *J. Am. Chem. Soc.* **2009**, *131*, 15939–15944.
27. Reddy, A. L. M.; Srivastava, A.; Gowda, S. R.; Gullapalli, H.; Dubey, M.; Ajayan, P. M. Synthesis Of Nitrogen-Doped Graphene Films for Lithium Battery Application. *ACS Nano* **2010**, *4*, 6337–6342.

28. Qian, W; Cui, X.; Hao, R.; Hou, Y.; Zhang, Z. Facile Preparation of Nitrogen-Doped Few-Layer Graphene *via* Supercritical Reaction. *ACS Appl. Mater. Interfaces* **2011**, *3*, 2259–2264.
29. Hong, J.-Y.; Shin, K.-Y.; Kwon, O. S.; Kang, H.; Jang, J. A Strategy for Fabricating Single Layer Graphene Sheets Based on a Layer-by-Layer Self-Assembly. *Chem. Commun.* **2011**, *47*, 7182–7184.
30. Sheng, Z.; Shao, L.; Chen, J.-J.; Bao, W.-J.; Wang, F.-B.; Xia, X.-H. Catalyst-Free Synhtesis of Nitrogen-Doped Graphene *via* Thermal Annealing Graphite Oxide with Mellamine and Its Excellent Electrocatalysts. *ACS Nano* **2011**, *5*, 4350–4358.
31. Wehling, T. O.; Novoselov, K. S.; Morozov, S. V.; Vdovin, E. E.; Katsnelson, M. I.; Geim, A. K.; Lichtenstein, A. I. Molecular Doping of Graphene. *Nano Lett.* **2008**, *8*, 173–177.
32. Long, D.; Li, W.; Ling, L.; Miyawaki, J.; Mochida, I.; Yoon, S.-H. Preparation of Nitrogen-Doped Graphene Sheets by a Combined Chemical and Hydrothermal Reduction of Graphene Oxide. *Langmuir* **2010**, *26*, 16096–16102.
33. Wang, S.; Yu, D.; Dai, L.; Chang, D. W.; Baek, J.-B. Polyelectrolyte-Functionalized Graphene as Metal-Free Electrocatalysts for Oxygen Reduction. *ACS Nano* **2011**, *5*, 6202–6209.
34. Jeon, I.-Y.; Yu, D.; Bae, X.-Y.; Choi, H.-J.; Chang, D. W.; Dai, L.; Baek, J.-B. Formation of Large-Area Nitrogen-Doped Graphene Film Prepared from Simple Solution Casting of Edge-Selectively Functionalized Graphite and Its Electrocatalytic Activity. *Chem. Mater.* **2011**, *23*, 3987–3992.
35. Deng, D.; Pan, X.; Yu, L.; Cui, Y.; Jiang, Y.; Qi, J.; Li, W.-X.; Fu, Q.; Ma, X.; Xue, Q.; *et al*. Toward N-Doped Graphene *via* Solvothermal Synthesis. *Chem. Mater.* **2011**, *23*, 1188–1193.
36. Xia, Y.; Walker, G. S.; Grant, D. M.; Mokaya, R. Hydrogen Storage in High Surface Area Carbons: Experimental Demonstration of the Effects of Nitrogen Doping. *J. Am. Chem. Soc.* **2009**, *131*, 16493–16499.
37. Guo, B.; Liu, Q.; Chen, E.; Zhu, H.; Fang, L.; Gong, J. R. Controllable N-Doping of Graphene. *Nano Lett.* **2010**, *10*, 4975–4980.
38. Wei, D.; Liu, Y.; Wang, Y.; Zhang, H.; Huang, L.; Yu, G. Synthesis of N-Doped Graphene by Chemical Vapor Deposition and Its Electrical Properties. *Nano Lett.* **2009**, *9*, 1752–1758.
39. Loureiro, R.; D'Amore, P. Transcriptional Regulation of Vascular Endothelial Growth Factor in Cancer. *Cytokine Growth Factor Rev.* **2005**, *16*, 77–89.
40. Foekens, J. A.; Peters, H. A.; Grebenchtchikov, N.; Look, M. P.; Gelder, M. E. M-V.; G-Moespot, A.; Kwast, T. H. V. D.; Sweep, C. G. J.; Klijn, J. G. M. High Tumor Levels of Vascular Endothelial Growth Factor Predict Poor Response to Systemic Therapy in Advanced Breast Cancer. *Cancer Res.* **2001**, *15*, 5407–5414.
41. Kwon, O. S.; Jang, J. A High-Performance VEGF Aptamer Functionalized Polypyrrole Nanotube Biosensor. *Biomaterials* **2010**, *31*, 4740–4748.
42. Sung, J.; Barone, P. W.; Kong, H.; Strano, M. S. Sequential Delivery of Dexamethasone and VEGF to Control Local Tissue Response for Carbon Nanotube Fluorescence Based Micro-Capillary Implantable Sensors. *Biomaterials* **2009**, *30*, 622–631.
43. Zhaoa, S.; Yang, W.; Lai, R. Y. A Folding-Based Electrochemical Aptasensor for Detection of Vascular Endothelial Growth Factor in Human Whole Blood. *Biosens. Bioelectron.* **2011**, *26*, 2442–2447.
44. Anderson, S. M.; Chen, T. T.; Iruela-Arispe, M. L.; Segura, T. The Phosphorylation of Vascular Endothelial Growth Factor Receptor-2 (VEGFR-2) by Engineered Surfaces with Electrostatically or Covalently Immobilized VEGF. *Biomaterials* **2009**, *30*, 4618–4628.
45. Tiedemann, B. V.; Bilitewski, U. Characterization of the Vascular Endothelial Growth Factor—Receptor Interaction and Determination of the Recombinant Protein by an Optical Receptor Sensor. *Biosens. Bioelectron.* **2002**, *17*, 983–991.
46. Jang, J.; Oh, J. H.; Stucky, G. D. Fabrication of Ultrafine Conducting Polymer and Graphite Nanoparticles. *Angew. Chem., Int. Ed.* **2002**, *41*, 4016–4019.
47. Jang, J.; Yoon, H. Fabrication of Magnetic Carbon Nanotubes Using a Metal-Impregnated Polymer Precursor. *Adv. Mater.* **2003**, *15*, 2088–2091.
48. Jang, J. Conducting Polymer Nanomaterials and Their Applications. *Adv. Polym. Sci.* **2006**, *199*, 189–259.
49. Jang, J.; Lim, B. Facile Fabrication of Inorganic-Polymer Core—Shell Nanostructures by a One-Step Vapor Deposition Polymerization. *Angew. Chem., Int. Ed.* **2003**, *42*, 5600–5603.
50. Das, A.; Pisana, S.; Chakraborty, B.; Piscanec, S.; Saha, S. K.; Waghmare, U. V.; Novoselov, K. S.; Krishnamurthy, H. R.; Geim, A. K.; Ferrari, A. C.; *et al*. Monitoring Dopants by Raman Scattering in an Electrochemically Top-Gated Graphene Transistor. *Nat. Nanotechnol.* **2008**, *3*, 210–215.
51. Ferrari, A. C.; Meyer, J. C.; Scardaci, V.; Casiraghi, C.; Lazzeri, M.; Mauri, F.; Piscanec, S.; Jiang, D.; Novoselov, K. S.; Roth, S.; *et al*. Raman Spectrum of Graphene and Graphene Layers. *Phys. Rev. Lett.* **2006**, *97*, 187401.
52. Yan, J.; Henriksen, E. A.; Kim, P.; Pinczuk, A. Observation of Anomalous Phonon Softening in Bilayer Graphene. *Phys. Rev. Lett.* **2008**, *101*, 136804.
53. Dong, X.; Shi, Y.; Huang, W.; Chen, P.; Li, L.-J. Electrical Detection of DNA Hybridization with Single-Base Specificity Using Transistors Based on CVD-Grown Graphene Sheets. *Adv. Mater.* **2010**, *22*, 1649–1653.
54. Gulbakan, B.; Yasun, E.; Shukoor, M. I.; Zhu, Z.; You, M.; Tan, X.; Sanchez, H.; Powell, D. H.; Dai, H.; Tan, W. A Dual Platform for Selective Analyte Enrichment and Ionization in Mass Spectrometry Using Aptamer-Conjugated Graphene Oxide. *J. Am. Chem. Soc.* **2010**, *132*, 17408–17410.
55. Chen, F.; Qing, Q.; Xia, J.; Li, J.; Tao, N. Electrochemical Gate-Controlled Charge Transport in Graphene in Ionic Liquid and Aqueous Solution. *J. Am. Chem. Soc.* **2009**, *131*, 9908–9909.
56. Willner, I.; Zayats, M. Electronic Aptamer-Based Sensors. *Angew. Chem., Int. Ed.* **2007**, *46*, 6408–6418.
57. Stine, R.; Robinson, J. T.; Sheehan, P. E.; Tamanaha, C. R. Real-Time DNA Detection Using Reduced Graphene Oxide Field Effect Transistors. *Adv. Mater.* **2010**, *22*, 5297–5300.
58. Chen, R. J.; Wang, Y.; Wang, D.; Dai, H. Noncovalent Sidewall Functionalization of Single-Walled Carbon Nanotubes for Protein Immobilization. *J. Am. Chem. Soc.* **2001**, *123*, 3838–3839.
59. Lee, L. M.; Heimark, R. L.; Baygents, J. C.; Zohar, Y. Self-Aligned Immobilization of Proteins Utilizing PEG Patterns. *Nanotechnology* **2006**, *17*, S29–33.
60. Yoon, H; Lee, S. H.; Kwon; Song, H. S.; Oh, E. H.; Park, T. H.; Jang, J. Polypyrrole Nanotubes Conjugated with Human Olfactroy Receptors: High-Performance Transducers for FET-Type Bioelectronic Noses. *Angew. Chem., Int. Ed.* **2009**, *48*, 2755–2758.
61. Zelada-Guill, G. A.; Riu, J.; Duzgun, A.; Rius, F. X. Immediate Detection of Living Bacteria at Ultralow Concentrations Using a Carbon Nanotube Based Potentiometric Aptasensor. *Angew. Chem., Int. Ed.* **2009**, *48*, 7334–7337.
62. Xiang, Y.; Xie, M.; Bash, R.; Chen, J. J. L.; Wang, J. Ultrasensitive Label-Free Aptamer-Based Electronic Detection. *Angew. Chem., Int. Ed.* **2007**, *46*, 9054–9056.
63. Ohno, Y.; Maehashi, K.; Matsumoto, K. Label-Free Biosensors Based on Aptamer-Modified Graphene Field-Effect Transistors. *J. Am. Chem. Soc.* **2010**, *132*, 18012–18013.
64. Willner, I.; Zayats, M. Electronic Aptamer-Based Sensors. *Angew. Chem., Int. Ed.* **2007**, *46*, 6408–6418.
65. So, H.; Won, K.; Kim, Y. H.; Kim, B.-K.; Ryu, B. H.; Na, P. S.; Kim, H.; Lee, J.-O. Single-Walled Carbon Nanotube Biosensors Using Aptamers as Molecular Recognition Elements. *J. Am. Chem. Soc.* **2005**, *127*, 11906–11907.
66. Song, S.; Wang, L.; Li, J.; Zhao, J.; Fan, C. Aptamer-Based Biosensors. *Trends Anal. Chem.* **2008**, *27*, 10–117.
67. Wei, P.; Oh, J. H.; Dong, G.; Bao, Z. Use of a 1*H*-Benzoimidazole Derivative as an *n*-Type Dopant and To Enable Air-Stable

Solution-Processed *n*-Channel Organic Thin-Film Transistors. *J. Am. Chem. Soc.* **2010**, *132*, 8852–8853.
68. Oh, J. H.; Wei, P.; Bao, Z. Molecular n-Type Doping for Air-Stable Electron Transport in Vacuum-Processed n-Channel Organic Transistors. *Appl. Phys. Lett.* **2010**, *97*, 243305.
69. Lee, H.-S.; Kim, K. S.; Kim, C.-J.; Hahn, S. K.; Jo, M.-H. Electrical Detection of VEGFs for Cancer Diagnoses Using Anti-Vascular Endotherial Growth Factor Aptamer-Modified Si Nanowire FETs. *Biosens. Bioelectron.* **2009**, *24*, 1801–1805.
70. Kim, K. S.; Zhao, Y.; Jang, H.; Lee, S. Y.; Kim, J. M.; Kim, K. S.; Ahn, J.-H.; Kim, P.; Choi, J.-Y.; Hong, B. H. Large-Scale Pattern Growth of Graphene Films for Stretchable Transparent Electrodes. *Nature* **2009**, *457*, 706–710.
71. Mcalpine, M. C.; Ahmad, H.; Wang, D.; Heath, J. R. Highly Ordered Nanowire Arrays on Plastic Substrates for Ultrasensitive Flexible Chemical Sensors. *Nat. Mater.* **2007**, *6*, 379–384.